Cell Reports
Report

Structural Insights into RIP3-Mediated Necroptotic Signaling

Tian Xie,[1,2] Wei Peng,[1,2] Chuangye Yan,[1] Jianping Wu,[1] Xinqi Gong,[1] and Yigong Shi[1,*]
[1]Ministry of Education Protein Science Laboratory, Tsinghua-Peking Joint Center for Life Sciences, Center for Structural Biology, School of Life Sciences and School of Medicine, Tsinghua University, Beijing 100084, China
[2]These authors contributed equally to this work
*Correspondence: shi-lab@tsinghua.edu.cn
http://dx.doi.org/10.1016/j.celrep.2013.08.044

SUMMARY

RIP3 is an essential upstream kinase in necroptosis. The pseudokinase MLKL functions as a substrate of RIP3 to mediate downstream signaling. The molecular mechanism by which RIP3 recognizes and phosphorylates MLKL remains unknown. Here, we report the crystal structures of the mouse RIP3 kinase domain, the MLKL kinase-like domain, and a binary complex between the two. Both RIP3 and MLKL adopt the canonical kinase fold. Free RIP3 exists in an active conformation, whereas MLKL-bound RIP3 is stabilized by AMP-PNP to adopt an inactive conformation. The formation of the RIP3-MLKL complex, involving their respective N- and C-lobes, is accompanied by pronounced conformational changes of the αC helix and activation loop in RIP3 and the corresponding structural elements in MLKL. RIP3-mediated MLKL phosphorylation, though important for downstream signaling, is dispensable for stable complex formation between RIP3 and MLKL. Our study serves as a framework for mechanistic understanding of RIP3-mediated necroptotic signaling.

INTRODUCTION

Necroptosis, also known as programmed necrosis, refers to death-receptor-initiated cell death under conditions where the execution of apoptosis is prevented (Christofferson and Yuan, 2010; Vandenabeele et al., 2010). Necroptosis is closely associated with diseases, exemplified by its role in the pathogenesis of ischemic injury, neurodegeneration, and viral infection (Vandenabeele et al., 2010). Consequently, understanding the molecular mechanisms of necroptosis is important for potential therapeutic intervention.

In response to tumor necrosis factor (TNF)-α activation, two conserved Ser/Thr protein kinases RIP1 (Stanger et al., 1995) and RIP3 (Sun et al., 1999; Yu et al., 1999) together form a multimeric complex, named necrosome, to initiate the necroptotic process (Cho et al., 2009; He et al., 2009). Both proteins contain an N-terminal kinase domain and a RIP homotypic interaction motif (RHIM) (Sun et al., 2002), and RIP1 also has an extra C-terminal death domain (Stanger et al., 1995). The kinase domains of RIP1 and RIP3 share 33% sequence identity and 53% sequence similarity, and the kinase activities of RIP1 and RIP3 are essential for TNF-α-induced necroptosis (Cho et al., 2009; He et al., 2009). The RHIM domains of RIP1 and RIP3 are thought to mediate homotypic interactions, facilitating formation of the RIP1-RIP3 necrosome required for necroptosis (Li et al., 2012; Sun et al., 2002). The mixed lineage kinase domain-like protein (MLKL) and the mitochondrial protein phosphatase PGAM5 were recently found to function downstream of RIP3 (Sun et al., 2012; Wang et al., 2012). The MLKL kinase-like domain was so named because it lacks the canonical ATP-binding P-loop, the catalytic loop, or the activation loop. RIP3 directly phosphorylates the pseudokinase MLKL at Thr357 and Ser358, which appears to be critical for necroptosis execution (Sun et al., 2012). Phosphorylation by RIP3 leads to enhanced phosphatase activity of PGAM5, which dephosphorylates Drp1 to mediate mitochondrial fragmentation and initiate necroptosis (Wang et al., 2012).

MLKL consists of an N-terminal coiled-coil domain and a C-terminal kinase-like domain. A small molecule named necrosulfonamide can be covalently linked to Cys86 of MLKL coiled-coil domain to block necrosis downstream of RIP3 activation (Sun et al., 2012). The C-terminal kinase-like domain of MLKL is responsible for association with RIP3 (Sun et al., 2012). Both RIP3 and MLKL are highly conserved, with 69%/77% sequence identity/similarity for the kinase domains of human and mouse RIP3, and 69%/81% sequence identity/similarity for the kinase-like domains of human and mouse MLKL.

Despite an essential role of RIP3 and MLKL in necroptosis, there is no atomic-resolution structure on either protein. The lack of structural information has hindered functional and mechanistic understanding of the RIP3 kinase-mediated MLKL phosphorylation and signaling. In this study, we present the crystal structures of the mouse RIP3 kinase domain, the mouse MLKL kinase-like domain, and the RIP3-MLKL complex. Our results reveal the structural and biochemical basis for the recognition and phosphorylation of MLKL kinase-like domain by RIP3 kinase domain.

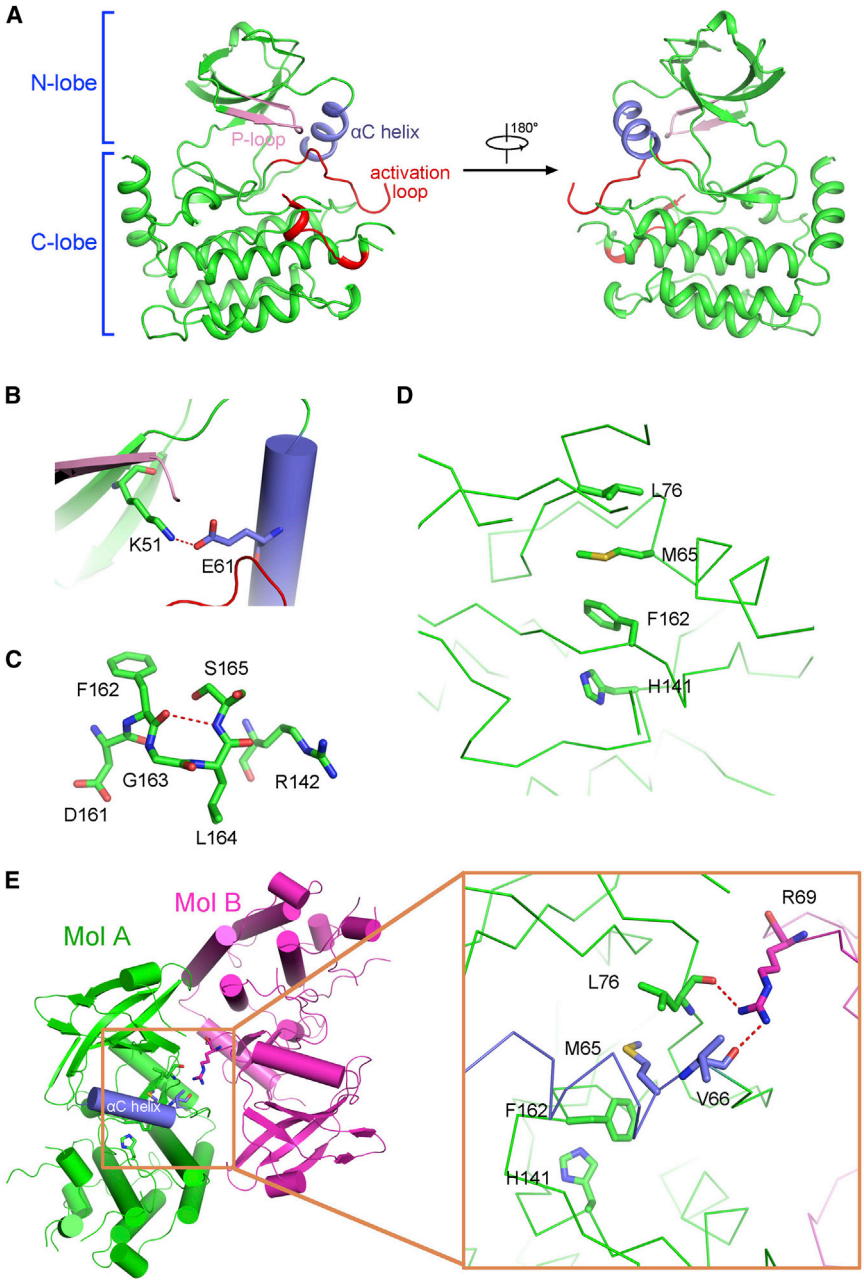

Figure 1. Overall Structure of the Mouse RIP3 Kinase Domain

(A) Overall structure of the mouse RIP3 kinase domain (colored green). The P-loop (residues 29–36) and the αC helix (residues 57–66) are colored pink and purple, respectively. The activation loop (residues 161–194) is highlighted in red; residues 171–185 are disordered in the crystals. All structural figures were prepared with PyMOL (DeLano, 2002).

(B) Lys51 forms a H-bond with Glu61 from the αC helix of RIP3. The side chains of Lys51 and Glu61 are shown in sticks. H-bonds in this and all other figures are represented by red dashed lines.

(C) H-bond between Phe162 and Ser165 of RIP3 helps to stabilize the DFG motif in the active configuration.

(D) The hydrophobic spine structure in RIP3. The side chains of the four amino acids, shown in sticks, stack against each other in a linear fashion.

(E) Crystal lattice packing interactions between two RIP3 molecules in an asymmetric unit. The side chain of Arg69 in one molecule (Mol B) makes two H-bonds to the main chain groups of Val66 and Leu76 in the other molecule (Mol A), and vice versa.

See also Figure S1.

RESULTS AND DISCUSSION

Overall Structure of the RIP3 Kinase Domain

We crystallized the mouse RIP3 kinase domain (residues 1–313) with a C111A mutation, which has no detectable impact on the kinase activity of RIP3 (data not shown) and determined its structure by molecular replacement using the atomic coordinates of human RIP1 kinase domain (Protein Data Bank [PDB] ID code 4ITH) (Xie et al., 2013). The atomic model was refined at 2.4 Å resolution (Figure 1A; Table S1).

There are two molecules of RIP3 kinase domain in each asymmetric unit. Because these two molecules display identical features relevant for discussion, we only focus on one such molecule. RIP3 exhibits a canonical kinase fold, with an N-lobe, a C-lobe, and an intervening activation loop (residues 161–194, also known as T-loop). The N-lobe comprises an antiparallel, five-stranded β-sheet and an activation helix (residues 57–66, commonly known as the αC helix) (Figures 1A and S1A). The C-lobe contains eight α-helices and a pair of β-strands. All essential amino acids for ATP binding and hydrolysis in canonical kinases are conserved in RIP3, including the catalytic triad residues Lys51/Glu61/Asp161 and key residues in the P-loop (residues 29–36) and catalytic loop (residues 141–148).

Structural comparison between RIP3 and the catalytic subunit of protein kinase A (PKA; PDB ID code 2CPK) (Knighton et al., 1991a, 1991b) suggests that the free RIP3 kinase domain adopts an active conformation (Figure S1B). The active kinase PKA contains a salt bridge between Lys72 and Glu91, which helps Lys72 to stabilize ATP through H-bonds to the α- and β-phosphates. Similarly, the corresponding amino acids Lys51 and Glu61 in the RIP3 kinase domain form a salt bridge (Figures 1B and S1B). In addition, the configuration of the Asp-Phe-Gly (DFG) motif in the activation loop of RIP3, which contains a conserved H-bond between carbonyl oxygen of Phe162 and amide nitrogen of Ser165 (the DFG + 2 residues) to help maintain the kinase in an active conformation, is quite similar to that in PKA (Kornev et al., 2006)

(Figures 1C and S1C). Furthermore, similar to other active protein Ser/Thr kinases (Kornev et al., 2006), RIP3 also contains an assembled hydrophobic spine structure in which four hydrophobic amino acids stack against each other in a spatially linear order (Figures 1D and S1D). This structural feature stabilizes the kinase fold and helps the kinase to go through open and closed conformations during catalysis (Kornev et al., 2006). The hydrophobic spine of RIP3 comprises Leu76, Met65, Phe162, and His141, which correspond to Leu106, Leu95, Phe185, and Tyr164, respectively, in PKA (Figures 1D and S1D).

The two molecules of RIP3 kinase domain in an asymmetric unit pack against each other and exhibit a pseudo 2-fold symmetry (Figure 1E). The side chain of Arg69 in one molecule donates two H-bonds to the main chains of Val66 and Leu76 in the other molecule, and vice versa (Figure 1E). These H-bonds may help to stabilize the αC helix and the hydrophobic spine, allowing the kinase to maintain an active conformation.

Formation of the RIP3-MLKL Complex and Phosphorylation of MLKL by RIP3

On the basis of cellular coimmunoprecipitation data, the kinase domain of RIP3 was reported to directly interact with the kinase-like domain of MLKL (Chen et al., 2013; Sun et al., 2012). We expressed and purified the mouse RIP3 kinase domain and the mouse MLKL kinase-like domain. However, the individually purified RIP3 kinase domain (RIP3-KD, residues 1–318) and MLKL kinase-like domain (MLKL-KL, residues 182–464) failed to form a stable complex as judged by gel filtration analysis (Figure 2A). Only when coexpressed together in insect cells, RIP3-KD and MLKL-KL formed a stable complex (Figure 2A). This result suggests that formation of the RIP3-MLKL complex may depend on specific phosphorylation states of these two proteins.

The binding of MLKL by RIP3 results in the phosphorylation of MLKL kinase-like domain in vivo (Chen et al., 2013; Sun et al., 2012). We sought to reconstitute an in vitro kinase activity assay of RIP3 toward MLKL and determine the MLKL phosphorylation sites (Figure 2B). Subsequent analysis by mass spectrometry (MS) revealed that Ser345, Ser347, Thr349, and Ser352 of MLKL kinase-like domain were phosphorylated by the RIP3 kinase domain (Figure S2A). These four phosphorylation sites in MLKL were further confirmed by in vitro kinase activity assay (Figure 2B). Single missense mutation in MLKL, involving any of the four potential phosphorylation residues Ser345/Ser347/Thr349/Ser352 to Ala or Glu, still allowed RIP3-mediated phosphorylation. By contrast, the quadruple mutants ST4A (S345A/S347A/T349A/S352A) and ST4E (S345E/S347E/T349E/S352E) completely abrogated RIP3-mediated phosphorylation. In addition, the MLKL quadruple variant ST4A or ST4E retained the ability to form a stable complex with coexpressed RIP3 (Figures S2B and S2C). Further data strongly suggest that additional phosphorylation of RIP3, instead of MLKL, is required for stable RIP3-MLKL complex formation (see the Extended Results and Discussion; Figures S2B–S2D).

We crystallized the mouse MLKL kinase-like domain (residues 182–464) and determined its structure by molecular replacement using the atomic coordinates of human MLKL kinase-like domain (which will be discussed later). The X-ray structure of the mouse MLKL kinase-like domain was refined at 1.6 Å resolution (Figure 2C; Table S1). Despite lack of the catalysis-related sequence elements, the mouse MLKL kinase-like domain displays a kinase fold with N- and C-lobes that are generally indistinguishable to other protein kinases. The N-lobe comprises an antiparallel, five-stranded β-sheet and an α-helix, whereas the C-lobe contains seven α-helices and a pair of β-strands (Figures 2C and S2E). All four residues that are phosphorylated by RIP3 are located at the intervening loop region between the N- and C-lobes of MLKL, of which two residues Ser345 and Ser347 were modeled on the basis of clear electron density.

Structure of the RIP3-MLKL Complex

To elucidate the mechanism of MLKL recognition and phosphorylation by RIP3, we sought to crystallize a binary complex between RIP3 and MLKL. After numerous trials, we were able to generate crystals of the complex between mouse RIP3 (residues 1–318) and mouse MLKL (residues 182–464) in the presence of 2 mM adenosine 5′-[β,γ-imido]triphosphate (AMP-PNP; a nonhydrolyzable ATP analog) in the $C222_1$ space group. The complex structure was determined by molecular replacement using the atomic coordinates of mouse MLKL kinase-like domain and mouse RIP3 kinase domain. The atomic model was refined to 2.5 Å resolution (Figures 3A and S3A; Table S1).

The mouse RIP3 kinase domain forms a 1:1 complex with the kinase-like domain of MLKL (Figure 3A). RIP3 and MLKL are aligned in a parallel fashion, with the N- and C-lobes of RIP3 packing closely against the N- and C-lobes of MLKL, respectively (Figures 3A, 3B, and S3A). Consequently, the RIP3-MLKL interface comprises two separate contact areas, one involving strands β1/β5 of RIP3 and α1/β4 of MLKL, and the other involving α7-α8 of RIP3 and α4-α6 of MLKL. The kinase-like domain of MLKL and the RIP3 kinase domain are related to each other by an approximate 90-degree rotation around a vertical axis. In addition, RIP3 is stabilized by an AMP-PNP molecule (Figures 3A and S3B). MS analysis showed that both RIP3 and MLKL are phosphorylated in the complex. The phosphorylation sites in RIP3 are clearly visible; however, the loop region between the N- and C-lobes of MLKL (residues 345–357), where the known phosphorylation sites are located, is disordered in the complex structure (Figure 3).

Interface between RIP3 and MLKL

The RIP3-MLKL interactions involve extensive van der Waals contacts and numerous H-bonds (Figures 3B–3E). At the center of the interface mediated by the N-lobes of RIP3 and MLKL, two phenyl rings from Phe27 of RIP3 and Phe234 of MLKL stack against each other through π-π interactions (Figure 3C). The importance of these π-π interactions is manifested by the greatly diminished association between RIP3 and MLKL as a consequence of the missense mutation F27E or F234E (Figure S3C). These π-π interactions are buttressed by van der Waals contacts between Phe87 of RIP3 and Val229/Ile259 of MLKL. In addition, the hydroxyl group of Ser228 in MLKL accepts a H-bond from the side chain of Lys56 in RIP3 and donates a H-bond to Ser89; the hydroxyl group of Thr235 in MLKL accepts a H-bond from the ε-amino group of Lys30 in RIP3 (Figure 3C).

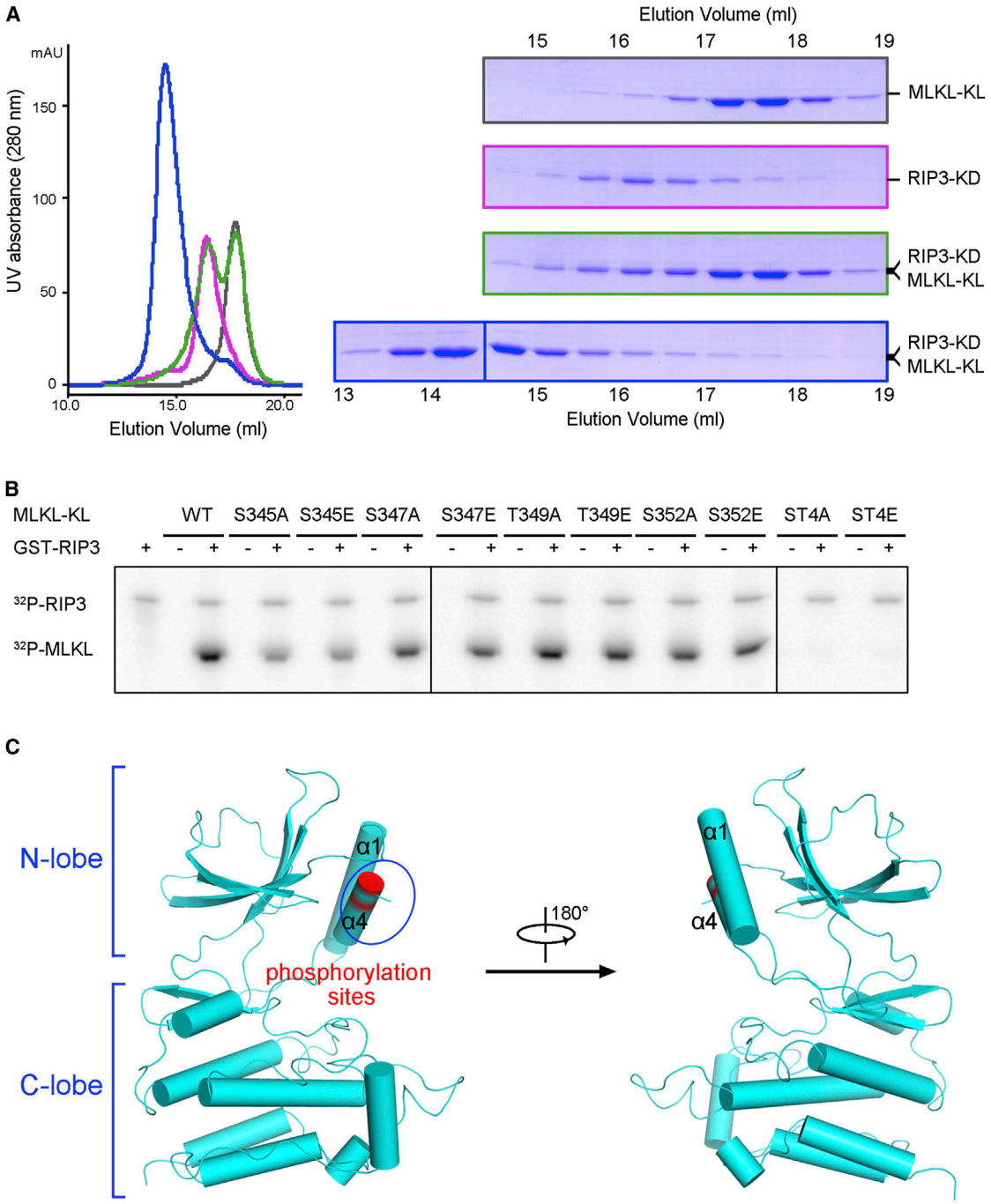

Figure 2. In Vitro Binding and Phosphorylation of MLKL by RIP3

(A) Analysis of the interactions between mouse RIP3 kinase domain (RIP3-KD) and mouse MLKL kinase-like domain (MLKL-KL) by gel filtration. The same elution fractions of each gel filtration run were applied to SDS-PAGE followed by Coomassie blue staining. Individually expressed and purified RIP3 and MLKL failed to form a stable complex, whereas coexpressed RIP3 and MLKL formed a stable complex.

(B) In vitro phosphorylation of wild-type and mutant MLKL by RIP3. MLKL was phosphorylated at Ser345, Ser347, Thr349, and Ser352. Mutation of any of these four residues to Ala or Glu still allowed phosphorylation by RIP3, whereas the quadruple mutants S345A/S347A/T349A/S352A (ST4A) and S345E/S347E/T349E/S352E (ST4E) failed to be phosphorylated.

(C) Overall structure of mouse MLKL kinase-like domain (colored cyan). The four phosphorylation sites by RIP3 are located at an intervening region between the N- and C-lobes of MLKL. Ser345 and Ser347 are colored red, and Thr349 and Ser352 are disordered and invisible.

See also Figure S2.

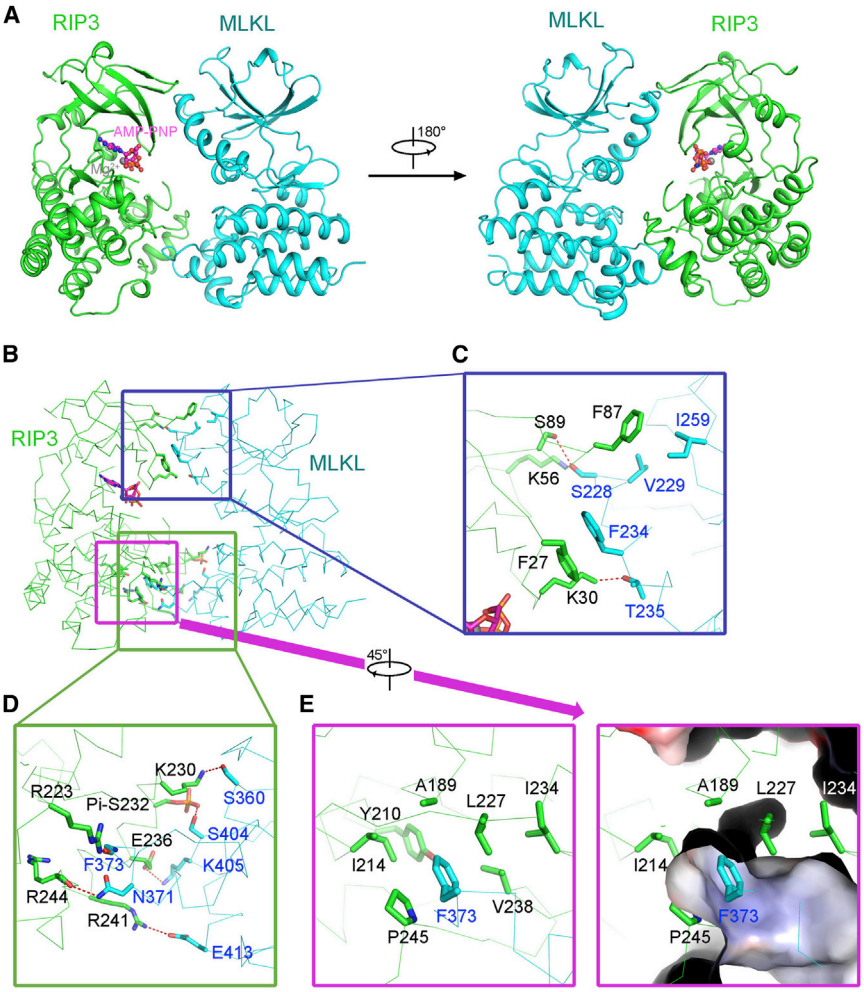

Figure 3. Structure of the Mouse RIP3-MLKL Complex and the Interface between RIP3 and MLKL

(A) Overall structure of the mouse RIP3-MLKL complex. The RIP3 kinase domain and MLKL kinase-like domain are colored green and cyan, respectively. AMP-PNP is shown in magenta ball and stick.

(B) The interface between the N- and C-lobes of RIP3 and MLKL. The interface residues are shown in sticks.

(C) A close-up view of the N-lobe interface between RIP3 and MLKL.

(D) A close-up view of the H-bond network in the C-lobe interface between RIP3 and MLKL.

(E) A close-up view of the hydrophobic interactions in the C-lobe interface between RIP3 and MLKL. The right panel shows the hydrophobic cavity surrounding Phe373 from MLKL.

See also Figure S3.

At the interface mediated by the C-lobes of RIP3 and MLKL, there are six discrete H-bonds and an area of concentrated van der Waals contacts. Notably, Ser232 appears to play an important role upon phosphorylation; the phosphate group of the phosphorylated Ser232 in RIP3 accepts a H-bond from the hydroxyl group of Ser404 in MLKL (Figure 3D). The side chains of Lys230, Glu236, and Arg241 in RIP3 each makes a H-bond to the side chains of Ser360, Lys405, and Glu413 in MLKL, respectively (Figure 3D). There are also two H-bonds involving the main chain groups, between Arg244 of RIP3 and Asn371 of MLKL, and between Arg223 of RIP3 and Phe373 of MLKL. Most notably, the phenyl ring of Phe373 in MLKL inserts into a hydrophobic pocket formed by the side chains of Ala189, Tyr210, Ile214, Leu227, Ile234, Val238, and Pro245 in RIP3 (Figure 3E).

To further corroborate the binding interface between RIP3 and MLKL, we performed mutational analysis. Consistent with a key role by the hydrophobic contacts, the mutation of Phe373 to Ala or Arg in MLKL led to complete disruption of the formation of RIP3-MLKL complex (Figure S3D). In addition, the mutation S404A in MLKL or the mutation S232A/S232D/S232E greatly attenuated formation of the RIP3-MLKL complex (Figure S3E). This result strongly suggests an important role by Ser232 phosphorylation in the formation of RIP3-MLKL complex, confirming an earlier observation (Sun et al., 2012). In contrast to the phosphorylation-dependent H-bond, other H-bonds appear to play a less important role, because disruption of an individual H-bond by K230A/E236A in RIP3 or K405 in MLKL had little impact on formation of the RIP3-MLKL complex (Figure S3E). Finally, as anticipated, the double mutations S404A/K405A in MLKL (SK2A) or the triple mutations K230A, S232A, and E236A in RIP3 (KSE3A) attenuated formation of the RIP3-MLKL complex (Figure S3E).

The human MLKL T357A/S358A mutant was previously reported to have a dominant-negative effect on necrosis (Sun et al., 2012). The corresponding phosphorylation site mutants of mouse MLKL (ST4A and ST4E) retained formation of the RIP3-MLKL complex (Figure S3F). This result suggests that physical association between RIP3 and MLKL is insufficient to mediate necrosis signaling and the RIP3-mediated phosphorylation of MLKL is crucial. Intriguingly, besides Ser232, two additional phosphorylated residues, Ser184 and Thr231 in RIP3, were observed in the RIP3-MLKL complex structure. Because Thr231 of RIP3 is not involved in the interface with MLKL, the mutation T231A/T231D/T231E had little impact on formation of the RIP3-MLKL complex (Figure S3G). Similar to S232A/S232D/S232E, the double mutations T231A/S232A (TS2A), T231D/S232D (TS2D), or T231E/S232E (TS2E) in RIP3 attenuated formation of the RIP3-MLKL complex (Figure S3G).

Inactive Conformation of MLKL-Bound RIP3

MLKL-bound RIP3 exhibits a root-mean-squared deviation (rmsd) value of 0.64 Å over 227 aligned Cα atoms with free RIP3 (Figure 4A). Despite the overall structural similarity,

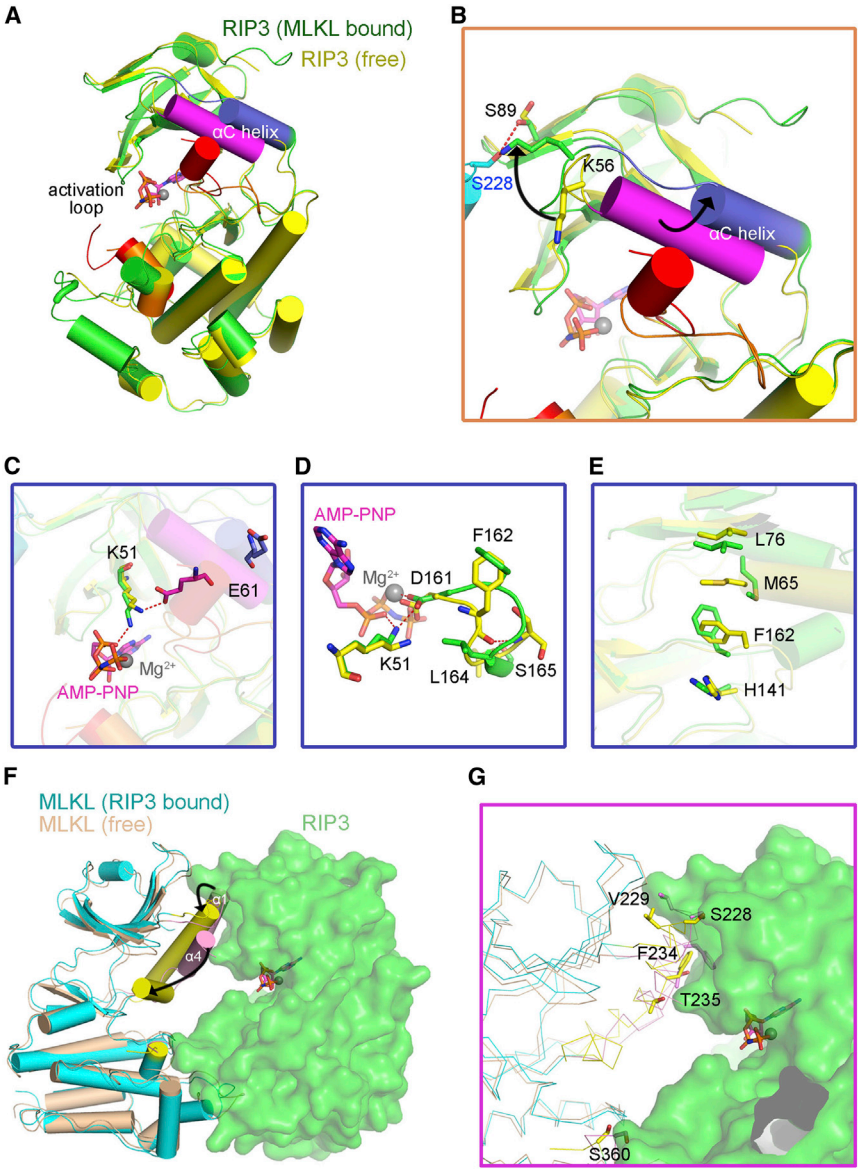

Figure 4. Conformational Changes of RIP3 and MLKL upon RIP3-MLKL Complex Formation

(A) Structural comparison of free RIP3 and MLKL-bound RIP3. Free RIP3 is colored yellow, with its αC helix in magenta and T-loop in orange. MLKL-bound RIP3 is colored green, with its αC helix in purple and T-loop in red. AMP-PNP is shown in magenta sticks.

(B) A close-up view of the conformational change in the N-lobe of RIP3 in response to MLKL binding. The side chains of Ser228 from MLKL and Lys56 and Ser89 from RIP3 are shown in sticks.

(C) The movement of αC helix leads to disruption of the salt bridge between Lys51 and Glu61 in RIP3.

(D) A close-up view of the conformational change in the DFG motif of RIP3 in response to MLKL binding.

(E) A close-up view of the rearrangement of the hydrophobic spine structure in RIP3 in response to MLKL binding.

(F) Structural comparison of free MLKL and RIP3-bound MLKL. Free MLKL is colored orange, with its α1 and α4 helices in pink. RIP3-bound MLKL is colored cyan, with its α1 and α4 helices in yellow. RIP3 is represented in green surface. AMP-PNP is shown in magenta sticks.

(G) A close-up view of the conformational changes of the residues in the N-lobe of MLKL in response to RIP3 binding. The residues are shown in sticks. See also Figure S4.

comparison between free RIP3 and MLKL-bound RIP3 reveals a drastic conformational change involving the αC helix and the activation loop (Figures 4A and 4B). Association with MLKL results in the formation of two H-bonds from the hydroxyl group of Ser228 in MLKL to the side chains of Lys56 and Ser89 in RIP3, of which Lys56 undergoes a pronounced rotation (Figure 4B). The αC helix is shifted by about 5 Å and its N-terminal portion is unwound (Figure 4B), moving Glu61 out of H-bond distance range of Lys51 (Figure 4C). Consequently, Glu61 is separated from Lys51 by about 16 Å, and the side chain of Lys51 donates a H-bond to the α-phosphate group of AMP-PNP (Figures 4C and S4A).

In addition to the rearrangement of αC helix in MLKL-bound RIP3, the DFG motif in the activation loop also adopts a different conformation, which is stabilized by a network of interactions involving AMP-PNP, the magnesium ion, and Lys51 (Figures 4D and S4A). Lys51 donates two H-bonds, one to Asp161 and the other to the α-phosphate group of AMP-PNP, whereas magnesium ion is coordinated by the side chain of Asp161 and the phosphate groups of AMP-PNP. Consequently, the conserved H-bond between the carbonyl oxygen of Phe162 and the amide nitrogen of Ser165 (the DFG + 2 residues), which helps maintain the kinase in an active conformation, is eliminated (Figure 4D). Due to reorientation of the αC helix and the activation loop, Met65 and Phe162 of the hydrophobic spine move away from their original positions, breaking the linear organization (Figure 4E). All these structural rearrangements together maintain MLKL-bound RIP3 in an inactive conformation.

The inactive conformation of MLKL-bound RIP3 is mainly stabilized by AMP-PNP, which is located in a pocket close to the P-loop and catalytic loop of RIP3 (see the Extended Results and Discussion; Figures S4A and S4B). Structural comparison of MLKL-bound RIP3 with a bisubstrate analog-bound tyrosine kinase ABL1 (Levinson et al., 2006) reveals that both the structures adopt the same local configurations to maintain the kinases in the inactive conformation and AMP-PNP in MLKL-bound RIP3 serves as an inhibitor to

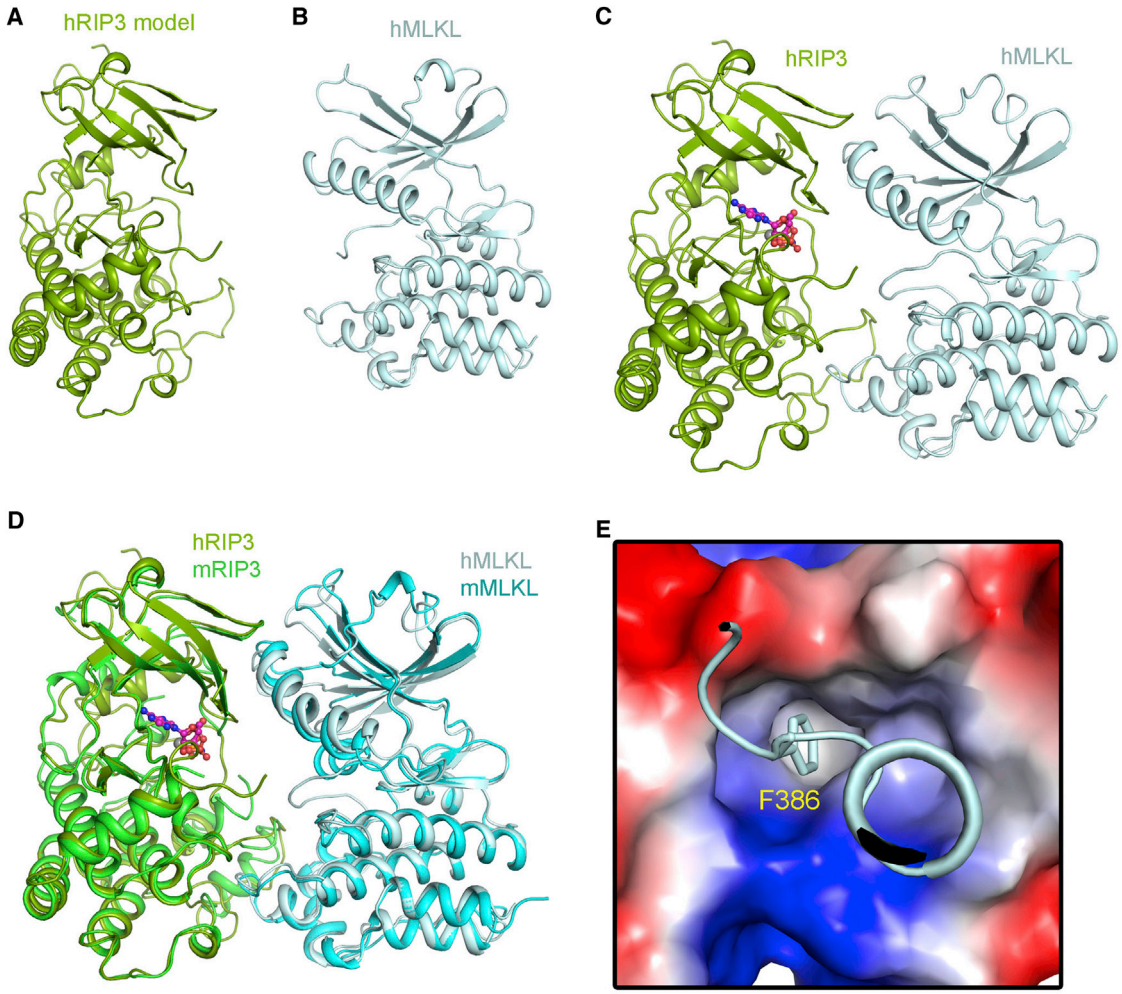

Figure 5. Homology Modeling of the Human RIP3-MLKL Complex

(A) A structural model of the human RIP3 kinase domain.

(B) The crystal structure of human MLKL kinase-like domain.

(C) A structural model of the human RIP3-MLKL complex. The human RIP3 and MLKL are colored dark green and light cyan, respectively.

(D) Structural comparison of the mouse RIP3-MLKL complex and the human RIP3-MLKL complex. The mouse RIP3 and MLKL are colored green and cyan, respectively. The human RIP3 and MLKL are colored dark green and light cyan, respectively.

(E) Phe386 in human MLKL inserts into a hydrophobic pocket in the C-lobe of human RIP3 on the basis of the modeled human RIP3-MLKL structure. The surface of human RIP3 is represented by electrostatic potential. Phe386 is shown in sticks.

See also Figure S5.

stabilize the RIP3-MLKL complex structure (see the Extended Results and Discussion; Figures S4C–S4E).

Conformational Changes of MLKL upon Binding to RIP3

RIP3-bound MLKL exhibits an rmsd value of 0.86 Å over 213 aligned Cα atoms with free MLKL (Figure 4F). Structural comparison between free MLKL and RIP3-bound MLKL reveals marked conformational changes in the α1 and α4 helices (Figure 4F), which correspond to the αC helix and the activation loop, respectively, in a canonical kinase. Due to steric clash, the binding of RIP3 leads to relocation of the α1 helix (residues 229–242) and the α4 helix and its ensuing loop (residues 336–360) in MLKL (Figure 4F). The movement of the α1/α4 helices and the loop following α4 results in rearrangement of the residues Ser228, Val229, Phe234, Thr235, and Ser360, which facilitates the interaction between RIP3 and MLKL (Figure 4G).

Homology Modeling of the Human RIP3-MLKL Complex

The human RIP3 kinase domain shares 69% sequence identity and 77% sequence similarity with the kinase domain of mouse RIP3 (Figure S1A). Using the programs Modeler 9.11 (Eswar et al., 2007) and JACKAL (Xiang et al., 2007), we generated a structural model for the human RIP3 kinase domain on the basis of the mouse RIP3 kinase domain structure (Figure 5A). In addition, we crystallized the human MLKL kinase-like domain and determined its structure by molecular replacement using the atomic coordinates of human RIP1 (PDB ID code 4ITH) (Xie et al., 2013). The atomic model was refined to a resolution of

1.9 Å (Figure 5B; Table S1). The human RIP3 kinase domain model and the human MLKL kinase-like domain structure were individually superimposed onto the structure of the mouse RIP3-MLKL complex; the resulting model was energy-minimized using the molecular dynamics package Gromacs 4.5 (Pronk et al., 2013) (Figure 5C).

As anticipated, the overall structure and interactions between the human and mouse RIP3-MLKL complexes are quite similar (Figure 5D). For example, Phe386 in human MLKL (corresponding to Phe373 in mouse MLKL) is surrounded by a highly conserved hydrophobic pocket in human RIP3 (Figure 5E). Consistent with the important role of Ser227 phosphorylation in human RIP3-MLKL complex formation, the phosphorylated Ser227 in human RIP3 (corresponding to Ser232 in mouse RIP3) accepts a H-bond from an invariable residue Ser417 in human MLKL (corresponding to Ser404 in mouse MLKL) (Figure S5A). Notably, the N- or C-lobe interface between RIP3 and MLKL contains a number of species-specific interactions, explaining the observation that human RIP3 and mouse MLKL, or mouse RIP3 and human MLKL, failed to form a stable complex (Chen et al., 2013; Sun et al., 2012). In the N-lobe interface of human RIP3-MLKL complex, the van der Waals contacts are greatly diminished, and the conserved Ser239 in human MLKL is predicted to form two H-bonds with two variable residues Asp87 and Lys89 in human RIP3 (Figure S5B). Similarly, the C-lobe interface H-bond network in human RIP3-MLKL complex is rearranged to fit the species-specific interface, involving the interactions mediated by the variable residues Glu225/Tyr230/Asn235/Ser241 in human RIP3 and Asp384/Gln388 in human MLKL (Figure S5A).

In summary, we report the crystal structures of the mouse RIP3 kinase domain, MLKL kinase-like domain, and RIP3-MLKL complex at atomic resolutions. Structural and biochemical analyses reveal the molecular basis for the RIP3-mediated recognition and phosphorylation of MLKL kinase-like domain. The phosphorylation of MLKL by RIP3 is crucial for downstream signaling. The phosphomimetic MLKL mutant, which remains associated with RIP3, was reported to retain the ability to induce necrosis (Sun et al., 2012). Together with this and other previous reports, our study indicates that the binding between RIP3 and MLKL is necessary, but not sufficient, for necrosis signaling. Disruption of the binding interface between RIP3 and MLKL prevents necroptosis downstream RIP3. Our structural and biochemical studies allow improved delineation of RIP3-mediated signaling events.

EXPERIMENTAL PROCEDURES

The recombinant RIP3 protein and MLKL protein were overexpressed in Sf-9 insect cells and *E. coli*, respectively. The mouse RIP3-MLKL complex was obtained by coexpression of RIP3 and MLKL in Sf-9 insect cells. All the proteins were purified to homogeneity and crystallized by the hanging-drop vapor-diffusion method. The data sets were collected at SPring-8 and Shanghai Synchrotron Radiation Facility (SSRF). All the data sets were processed with the HKL2000 (Otwinowski and Minor, 1997) and the CCP4 suite (Collaborative Computational Project, 1994). The structures were determined by molecular replacement using PHASER (McCoy et al., 2007). Manual model rebuilding and refinement were iteratively performed with COOT (Emsley and Cowtan, 2004) and PHENIX (Adams et al., 2002), respectively. The gel filtration analyses were performed to detect RIP3 and MLKL binding. The in vitro kinase activity assay was used to detect the kinase activity of RIP3 toward MLKL. Mass spectrometry analysis were performed to determine the phosphorylation sites in RIP3 and MLKL.

See the Extended Experimental Procedures for details.

ACCESSION NUMBERS

The atomic coordinates and structure factor files of human MLKL, mouse RIP3, MLKL, and RIP3-MLKL complex have been deposited in the Protein Data Bank under the accession numbers 4M67, 4M66, 4M68, and 4M69, respectively.

SUPPLEMENTAL INFORMATION

Supplemental Information includes Extended Results and Discussion, Extended Experimental Procedures, five figures, and one table and can be found with this article online at http://dx.doi.org/10.1016/j.celrep.2013.08.044.

ACKNOWLEDGMENTS

We thank J. He and Q. Wang at the Shanghai Synchrotron Radiation Facility beamline BL17U and the staff at the SPring-8 beamline BL41XU for assistance. This work was supported by funds from National Natural Science Foundation of China projects 31130002 and 31021002 and the Ministry of Science and Technology (grant number 2009CB918801).

Received: July 3, 2013
Revised: August 3, 2013
Accepted: August 27, 2013
Published: October 3, 2013

REFERENCES

Adams, P.D., Grosse-Kunstleve, R.W., Hung, L.W., Ioerger, T.R., McCoy, A.J., Moriarty, N.W., Read, R.J., Sacchettini, J.C., Sauter, N.K., and Terwilliger, T.C. (2002). PHENIX: building new software for automated crystallographic structure determination. Acta Crystallogr. D Biol. Crystallogr. *58*, 1948–1954.

Chen, W., Zhou, Z., Li, L., Zhong, C.Q., Zheng, X., Wu, X., Zhang, Y., Ma, H., Huang, D., Li, W., et al. (2013). Diverse sequence determinants control human and mouse receptor interacting protein 3 (RIP3) and mixed lineage kinase domain-like (MLKL) interaction in necroptotic signaling. J. Biol. Chem. *288*, 16247–16261.

Cho, Y.S., Challa, S., Moquin, D., Genga, R., Ray, T.D., Guildford, M., and Chan, F.K. (2009). Phosphorylation-driven assembly of the RIP1-RIP3 complex regulates programmed necrosis and virus-induced inflammation. Cell *137*, 1112–1123.

Christofferson, D.E., and Yuan, J. (2010). Necroptosis as an alternative form of programmed cell death. Curr. Opin. Cell Biol. *22*, 263–268.

Collaborative Computational Project, Number 4. (1994). The CCP4 suite: programs for protein crystallography. Acta Crystallogr. D Biol. Crystallogr. *50*, 760–763.

DeLano, W.L. (2002). The PyMOL Molecular Graphics System. http://www.pymol.org.

Emsley, P., and Cowtan, K. (2004). Coot: model-building tools for molecular graphics. Acta Crystallogr. D Biol. Crystallogr. *60*, 2126–2132.

Eswar, N., Webb, B., Marti-Renom, M.A., Madhusudhan, M.S., Eramian, D., Shen, M.Y., Pieper, U., and Sali, A. (2007). Comparative protein structure modeling using MODELLER. Curr. Protoc. Protein Sci. *2*, 2.9.

He, S., Wang, L., Miao, L., Wang, T., Du, F., Zhao, L., and Wang, X. (2009). Receptor interacting protein kinase-3 determines cellular necrotic response to TNF-alpha. Cell *137*, 1100–1111.

Knighton, D.R., Zheng, J.H., Ten Eyck, L.F., Ashford, V.A., Xuong, N.H., Taylor, S.S., and Sowadski, J.M. (1991a). Crystal structure of the catalytic subunit of

cyclic adenosine monophosphate-dependent protein kinase. Science *253*, 407–414.

Knighton, D.R., Zheng, J.H., Ten Eyck, L.F., Xuong, N.H., Taylor, S.S., and Sowadski, J.M. (1991b). Structure of a peptide inhibitor bound to the catalytic subunit of cyclic adenosine monophosphate-dependent protein kinase. Science *253*, 414–420.

Kornev, A.P., Haste, N.M., Taylor, S.S., and Eyck, L.F. (2006). Surface comparison of active and inactive protein kinases identifies a conserved activation mechanism. Proc. Natl. Acad. Sci. USA *103*, 17783–17788.

Levinson, N.M., Kuchment, O., Shen, K., Young, M.A., Koldobskiy, M., Karplus, M., Cole, P.A., and Kuriyan, J. (2006). A Src-like inactive conformation in the abl tyrosine kinase domain. PLoS Biol. *4*, e144.

Li, J., McQuade, T., Siemer, A.B., Napetschnig, J., Moriwaki, K., Hsiao, Y.S., Damko, E., Moquin, D., Walz, T., McDermott, A., et al. (2012). The RIP1/RIP3 necrosome forms a functional amyloid signaling complex required for programmed necrosis. Cell *150*, 339–350.

McCoy, A.J., Grosse-Kunstleve, R.W., Adams, P.D., Winn, M.D., Storoni, L.C., and Read, R.J. (2007). Phaser crystallographic software. J. Appl. Cryst. *40*, 658–674.

Otwinowski, Z., and Minor, W. (1997). Processing of X-ray diffraction data collected in oscillation mode. Methods Enzymol. *276*, 307–326.

Pronk, S., Páll, S., Schulz, R., Larsson, P., Bjelkmar, P., Apostolov, R., Shirts, M.R., Smith, J.C., Kasson, P.M., van der Spoel, D., et al. (2013). GROMACS 4.5: a high-throughput and highly parallel open source molecular simulation toolkit. Bioinformatics *29*, 845–854.

Stanger, B.Z., Leder, P., Lee, T.H., Kim, E., and Seed, B. (1995). RIP: a novel protein containing a death domain that interacts with Fas/APO-1 (CD95) in yeast and causes cell death. Cell *81*, 513–523.

Sun, X., Lee, J., Navas, T., Baldwin, D.T., Stewart, T.A., and Dixit, V.M. (1999). RIP3, a novel apoptosis-inducing kinase. J. Biol. Chem. *274*, 16871–16875.

Sun, X., Yin, J., Starovasnik, M.A., Fairbrother, W.J., and Dixit, V.M. (2002). Identification of a novel homotypic interaction motif required for the phosphorylation of receptor-interacting protein (RIP) by RIP3. J. Biol. Chem. *277*, 9505–9511.

Sun, L., Wang, H., Wang, Z., He, S., Chen, S., Liao, D., Wang, L., Yan, J., Liu, W., Lei, X., and Wang, X. (2012). Mixed lineage kinase domain-like protein mediates necrosis signaling downstream of RIP3 kinase. Cell *148*, 213–227.

Vandenabeele, P., Galluzzi, L., Vanden Berghe, T., and Kroemer, G. (2010). Molecular mechanisms of necroptosis: an ordered cellular explosion. Nat. Rev. Mol. Cell Biol. *11*, 700–714.

Wang, Z., Jiang, H., Chen, S., Du, F., and Wang, X. (2012). The mitochondrial phosphatase PGAM5 functions at the convergence point of multiple necrotic death pathways. Cell *148*, 228–243.

Xiang, Z., Steinbach, P.J., Jacobson, M.P., Friesner, R.A., and Honig, B. (2007). Prediction of side-chain conformations on protein surfaces. Proteins. Structure, Function, and Bioinformatics *66*, 814–823.

Xie, T., Peng, W., Liu, Y., Yan, C., Maki, J., Degterev, A., Yuan, J., and Shi, Y. (2013). Structural basis of RIP1 inhibition by necrostatins. Structure *21*, 493–499.

Yu, P.W., Huang, B.C., Shen, M., Quast, J., Chan, E., Xu, X., Nolan, G.P., Payan, D.G., and Luo, Y. (1999). Identification of RIP3, a RIP-like kinase that activates apoptosis and NFkappaB. Curr. Biol. *9*, 539–542.